Earthquake Engineering, Tenth World Conference © 1992 Balkema, Rotterdam. ISBN 90 5410 060 5

Inelastic seismic response of pile supported bridge piers

Z. Feng & X. Zhu
Lanzhou Railway College, People's Republic of China

ABSTRACT: An overall inelastic seismic response analytical model is presented in this paper, in which both the material and geometric non–linearity are included, and the seismic response of an existing reinforced concrete pile supported railroad bridge pier, which was seriously damaged during the Haichen 1975 earthquake, was evaluated by using this model to check the accuracy and efficiency. The evaluation results have good agreements with the actual seismic damage appearances.

1 INTRODUCTION

Great efforts and progresses have been made about the seismic damage mechanism of bridges. The research results indicated that the most often occurred damages to the bridges during earthquakes are: tilting, settlement, sliding, cracking and overturning caused by liquefaction, excessive lateral seismic earth pressure et al; relative displacement of girders at supports and anchor bolt failures that resulted in "loss–of–span" at the piers and abutments. Problems still exist, especially about the effect of foundation to damage mechanism of bridges. The seismic damage mechanism of pile supported bridges are discussed in this paper.

Pile foundations have been widely used in bridge foundations. Pile as a bending member during earthquake, it is difficulty to evaluate its lateral resistant ability. There are many formulae can be used, but no two formulae can give the same results. On the other hand, almost all of the formulae were defined only for single pile, but most of the existing pile foundations are composed of at least two piles. The pile is in high stress condition under alternative load action during earthquakes. When the amplitude of the earthquake acceleration exceeded 0.1g, the effect of seismic loadings is one of the most important factors that should be considered in the design of bridges.

The objective of this study is to set up an overall inelastic seismic response analytical model and to check the accuracy and efficiency of this model through the seismic response evaluation of an existing pile supported railroad bridge, which was seriously damaged in the past earthquake.

2 DISCRETIZATION

In this analytical model, the two dimensional 4–node isoparametric quadrilateral elements are used in the discretization of soil. The Mohr–Coulomb criterion coupled with limited tension model is used to trace the non–linear behavior.

The Euler–Bernoulli cubic Hermitian beam elements are used to discretize the reinforced concrete members. The bearing is modelled by a beam element with a rigid end. The platform is modelled by rigid beam elements. An inelastic model in which both material and geometric non–linearity are included is used to represent the inelastic behavior. The Sina hysteresis model is used to trace the hysteresis pattern of the reinforced concrete members.

Since stress and strain in the soil will attain high values in the neighhood of the piles during the seismic excitation, the possibility of the separation and sliding between soil and piles is most likely along the interface between them. In this analysis, the Goodman's joint element is adopted to approach the separation and sliding behavior. The joint elements are set along the interfaces between soil and pile as well as soil and platform.

Several approaches have been used to date to approach the unbounded continua, but most of them are so complicated to be used in practical analysis. The traditional engineering approach of simple truncation introduces problems of positioning the finite boundary for accurate solution. In this analysis, the improved mapped infinite element (Feng et al 1986, 1987) coupled with conventional isoparametric element are used to approach the unbounded soil in the lateral direction. In this improved mapped infinite element, the linear type decay is defined.

In this study, it is assumed that only the displacement is compatible between various types elements and only single pier mode is used. The elements mesh scheme in longitudinal direction is shown in Fig.1.

3 ANALYTICAL MODEL FOR NON–LINEAR DYNAMIC ANALYSIS

An overall inelastic analytical model is presented in this paper, in which both geometric and material non–linearity are included. Soil–pile–pier interaction,

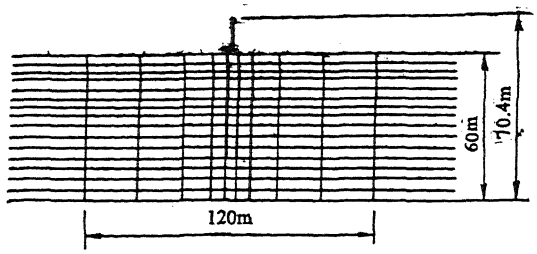

Fig.1 Elements mesh scheme in longitudinal direction

separation and sliding between them are also included. For reinforced concrete members, a detailed inelastic analytical model which include the buckling effect and hysteresis mechanism is presented.

3.1 Constitutive relationship of soil

It is assumed that the foundation soil is in plane stress condition. The Mohr–Coulomb yield criterion and the associated flow rule as well as limited tension model are coupled together for modelling the inelastic behavior of soil, in which the uniaxial stress–strain relation of soil can be defined as multilineal.

The Mohr–Coulomb yielding criterion can be expressed as(Fig.2):

$$\tau = c - \sigma_n tg\varphi, \tag{1}$$

or

$$\sigma_1 - \sigma_3 = 2c\cos\varphi - (\sigma_1 + \sigma_3)\sin\varphi, \tag{2}$$

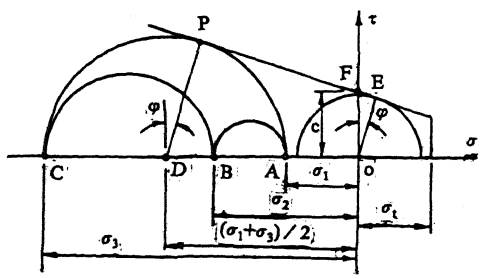

Fig.2 Mohr–Coulomb yield criterion

where τ is the magnitude of the shearing stress,$\sigma_n$is the normal stress, c is the cohesion and φ the angle of internal friction. The elasto–plastic incremental stress–strain relation can be written as:

$$d\sigma = D_{ep} d\varepsilon, \tag{3}$$

and

$$D_{ep} = D - \frac{d_0 d_D^T}{H' + d_D^T a}, \quad d_D^T = Da, \tag{4}$$

where D is the elastic stress–strain matrix. a is the flow vector. H' is work– hardening parameter and is obtained to be the local slope of the uniaxial stress–plastic strain curve.

liquefaction of the saturated sands during earthquake has been the cause of much damage to bridges. The effect of liquefaction of saturated sands is taken into account in this study. The judgement of liquefaction is based on the criterion stipulated by the China <Design Specification of Earthquake–resistant Buildings> (GBJ11–89). The calculated liquefaction index indicated that this site has heavy liquefaction grade and in this analysis, the liquefied soil layers have a different discount in Young's modulus, cohesion and frictional angle 1 / 2 to 1 / 3 according to the liquefaction index.

3.2 Analytical model for joint element

The joint element constructed from four nodal points. Two pairs of nodal points are assumed to occupy the same coordinate at initial state. The behavior of the contact surface between soil and substructure is expressed by relative position between surfaces of the joint element.

The deformation characteristics of the joint element are determined by the stiffness of the shear direction K_s and the normal direction K_n. The stress–strain characteristic of the joint element are assumed as shown in Fig.3 for the normal and shear component. The yield shear stress σ_y is determined as a function of the normal stress obeying the Mohr–coulomb failure law.

$$\begin{aligned} &\tau = c - \sigma_n tg\varphi \quad for\varepsilon_0 < 0, \\ &\tau = 0 \qquad\quad for\varepsilon_0 \geqslant 0. \end{aligned} \tag{5}$$

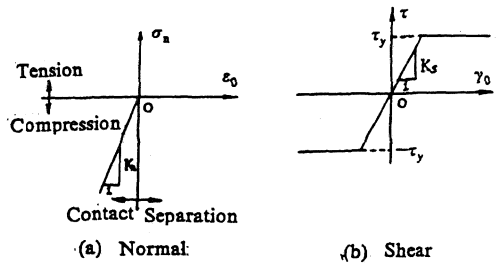

(a) Normal (b) Shear

Fig.3 Stress–strain relationship at midpointof the joint element

The normal stress is not transmitted for $\varepsilon_0 > 0$ and the linear constitutive relation based on the stiffness K_n is valid for $\varepsilon_0 < 0$. Spring coefficients K_n, K_s are related to the fictitious relative displacement of the interface between soil and substructure, which in actual response would not occur. Therefore, the spring coefficient should be as large as possible. However, numerical instability determines that their magnitude should be nearly equal to the stiffness of the substructure. Sliding will take place when the absolute value of shear stress reaches the yield shear stress τ_y, and the linear shear stress–strain relation remain below this stress lever. When separation occurs, the shear stress is not transmitted through the joint wall.

3.3 Analytical model for reinforced concrete member

The total deformation of the beam element includes four components, i.e. (1) elastic deformation; (2) inelastic deformation; (3) shear deformation and (4) geometric non–linear deformation.

The inelastic deformation is calculated by a procedure, first introduced by Otani(1972), which considers the element as two cantilevers with fixed ends at the supports and free ends at the point of contraflexure of the moment diagram(Fig.4).

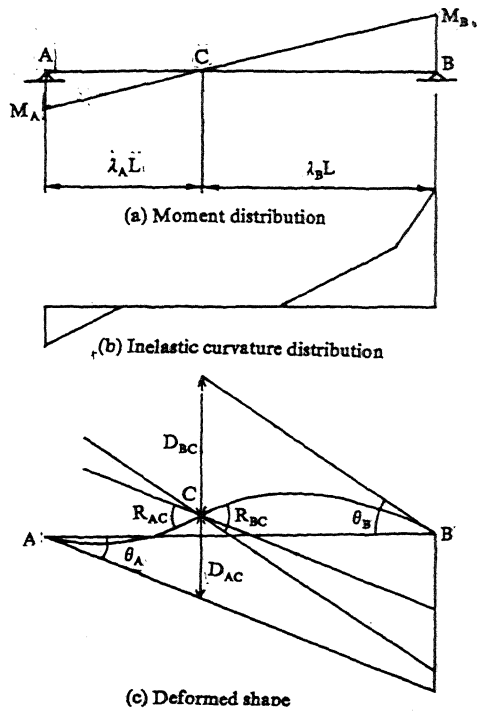

Fig.4 Geometry of member due to inelastic curvature.

The contribution of inelastic deformation to the flexibility can be written as:

$$\begin{bmatrix} \Delta\theta_A \\ \Delta\theta_B \end{bmatrix} = \begin{bmatrix} f_{11} & f_{12} \\ f_{21} & f_{22} \end{bmatrix} \begin{bmatrix} \Delta M_A \\ \Delta M_B \end{bmatrix}, \qquad (6)$$

where

$$f_{11} = \lambda_A L\left(\frac{\lambda_A}{SD(M_A)} + \frac{\lambda_B}{SR(M_A)}\right); \qquad (7a)$$

$$f_{12} = \lambda_B^2 L\left(\frac{1}{SD(M_B)} - \frac{1}{SR(M_B)}\right); \qquad (7b)$$

$$f_{21} = \lambda_A^2 L\left(\frac{1}{SD(M_A)} - \frac{1}{SR(M_A)}\right); \qquad (7c)$$

$$f_{22} = \lambda_B L\left(\frac{\lambda_B}{SD(M_B)} + \frac{\lambda_A}{SR(M_B)}\right); \qquad (7d)$$

in which

$$\lambda_A = \frac{M_A}{M_A + M_B}, \qquad (8)$$

$$\lambda_A + \lambda_B = 1, \qquad (9)$$

where $SD(M)$ and $SR(M)$ are the slopes of the moments vs. free end displacement and moment vs. free end rotation of unit length cantilever at moment M respectively.

It is noted that if $M_A \neq M_B$, f_{12} and f_{21} are not equal. Therefore, the flexibility matrix given by Eq.7a–7c is not symmetric in general. A symmetrization procedure of transfer diagonal entry is used in this analysis, which can be written as:

$$k_{ii} = k_{ii} - \sum_{j=1}^{i-1}\left[(k_{ij} - k_{ji})\frac{\delta_j}{\delta_i}\right], \quad (i = 2,\cdots,n) \qquad (10)$$

where k_{ii} is the diagonal entry of element stiffness, δ_i is the element nodal displacement and n is the degree of freedom of element. Iteration are required to solve Eq.10. Since the subject is non–linear, iteration has to be always performed and there is no penalty for symmetrization. This process has been proved to converge very fast and symmetrization can be done at the element lever.

Since the effect of liquefaction, the top sands layers will loss their resistant ability. The buckling stability of pile should be considered in such case. In this analytical model, this effect is taken into account by introducing the concept of stability functions (Harrison 1973) which are expressed in terms of the member axial force. A set of five stability functions are multiplied to the corresponding terms of stiffness matrix to modify the element stiffness in local coordinate. Besides, the geometry stiffness is added to the total element stiffness.

For reinforced concrete members, a detailed hysteresis model is desired that includes at least a trilinear loading curve as well as stiffness degradation. In this study, a modified version of the Takeda model is used. The model is known as the Sina model and is modified from the Takeda model by adding a "pinching" effect and simplifying the model by eliminating same of the rules. The inclusion of the pinching stiffness is found to improve the low amplitude response of the analytical models compared to experimental tests, however it also gives a large maximum displacement. The trilinear Sina model is shown in Fig.5. In which, nine rules regarding the loading, load reversal and unloading are defined. The pinching stiffness is not used by specifying a large pinching moment in this analysis. It was assumed that the hysteresis patten are not changed with the varying of axial load. The skeleton curve of load–deformation relationship is calculated by using elasto– plastic cracking Timoshenko layered beam model, in which the inelastic deformation, the shear deformation, the axial deformation and P–Δ effect are included(Feng et al 1991). The calculated fixed

end moment and free end displacement relation of unit length cantilever and idealized curves are shown in Fig.6. The axial load is taken as a constant(800kN) and is equal to the axial force under dead load plus 50% live load action.

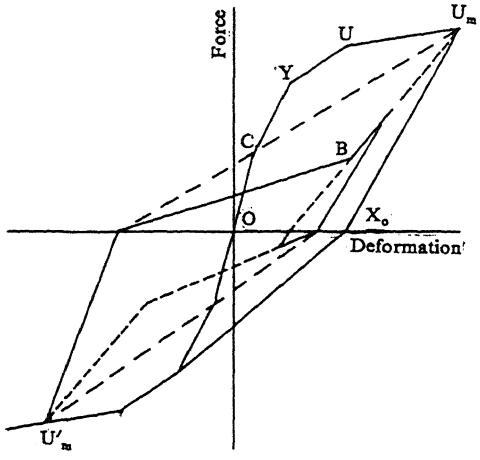

Fig.5 Sina hysteresis rules

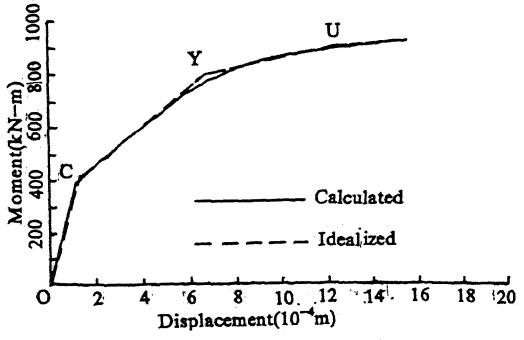

Fig.6 Load–deformation relationship of pile

5 EVALUATION OF SEISMIC RESPONSE

Daliao River Bridge was seriously damaged during the Haichen 1975 earthquake(M7.3). The earthquake intensity of this area is 7 degree. One of the most seriously damaged piers(No.15) of this railroad bridge moved 0.35m in the longitudinal direction after the earthquake. Most of the anchor bolts were broken and the bearing had a 0.35m relative displacement. The ground boiling and mudspouting was taken place during the earthquake. The postearthquake investigation revealed that the concrete of the pile body near the platform was heavily crushed. This pier is supported by six reinforced concrete piles in pre–bored holes. The length of pile is 43m and diameter 1.1m. The steel ratio is 0.6%. The element mesh scheme of pier No.15 is shown in Fig.1. A full span weight(342t) related to the pier is set on the top of the pier.

Since the initial stress distribution plays a very important role in the dynamic response analysis, the construction procedures are simply imitated in this study, in which it is assumed that the weight of supstructure is mainly sustained by the interface friction between pile and soil. The liquefaction is assumed to take place within 15m below the ground surface.

The Newmark's Beta integration algorithm with $\beta = 1/4$ is adopted in the time history analysis, the time interval is 0.005$sec.$ and the duration is 20$sec.$(4000 steps). In the numerical integration, 1–point Gauss–Legendre rule is used. The Newton–Raphson method is used in non–linear stress iteration. The convergence criterion based on energy is used to regard the convergence. The convergence tolerance is 0.2%. The global stiffness matrix is reconstructed at a certain step to accelerate the convergence.

The damping matrix [C] is constructed as the linear combination of the mass matrix [M] and stiffness matrix [K] as follows:

$$[C] = \alpha[M] + \beta[K] \tag{11}$$

The coefficients α and β are defined as:

$$\alpha = \frac{2(\xi_1\omega_3 - \xi_3\omega_1)}{(\omega_3 + \omega_1)(\omega_3 - \omega_1)}, \tag{12a}$$

$$\beta = \frac{2(\xi_3\omega_3 - \xi_1\omega_1)}{(\omega_3 + \omega_1)(\omega_3 - \omega_1)}, \tag{12b}$$

where ω_i is the ith natural frequency of the system and ξ_i is the damping factor for the ith mode.

The NS and UD components of the El Centro 1940 earthquake record are used as one of the ground motions for this analysis through inverse analysis by using the viscoelastic shear wave propagation formulae. The peak value of the accelerograph are scaled to 0.07g. Its predominant period are also adjusted. The computed horizontal ground motion response spectrum is shown in solid line in Fig.7. The original UD components are used with no changes except the peak values are scaled

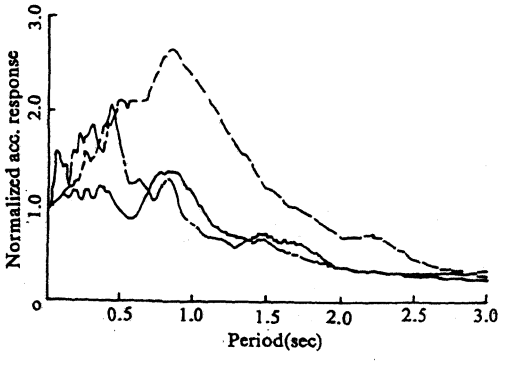

Fig.7 Normalized standard acceleration response spectrum of the ground motions

to 2 / 3 of the horizontal motion.

The calculated horizontal displacement time history of pier cap is shown in Fig.8. The maximum displacements is 2.74*cm*. The shear force acting at the bearing time diagram and shear force acting on the pier base time diagram are shown in Fig.9 and Fig.10. The maximum shear forces are 2210*kN* and 553*kN* respectively. It can be seen that the shear force acting at the bearing is much great than on the pier base.

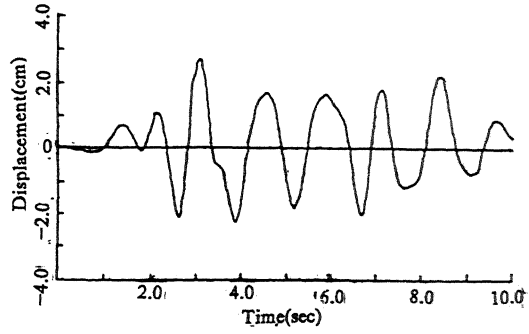

Fig.8 Horizontal displacement time diagram ofpier cap in longitudinal direction

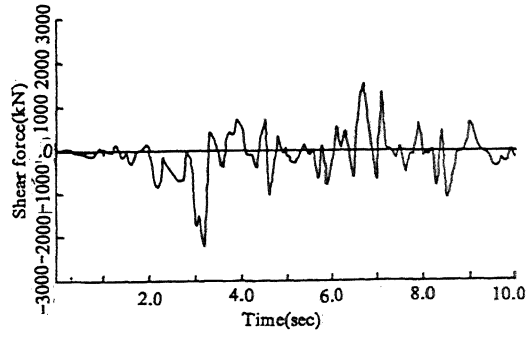

Fig.9 Shear force time diagram of bearing

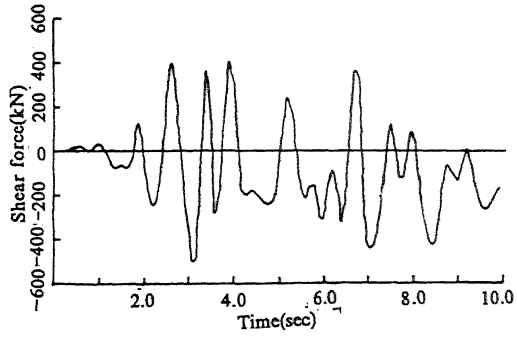

Fig.10 Shear force time diagram of pier base

Fig.11 shows the moment distribution along the pile. The maximum value in one of the pile reaches 870*kN–m*, approximately equal to the ultimate strength of 900*kN–m*. It is noted that the maximum value occurred at the pile end adjacent to platform and is much great than any other part in the pile. It is also noted that the degradation due to load repetition is severe and deterioration after yielding strength is drastic in this pile foundation because the pile has a low steel ratio(0.6%). The pile failure is caused by the degradation and deteriorating effect under the alternative seismic loadings. Since this pier is short, the calculated maximum moment at the pier base is under the cracking lever.

The calculated free site maximum acceleration at the ground surface is 0.12*g*.It matches the earthquake intensity of this site during the Haichen 1975 earthquake. The calculated maximum acceleration at the pier cap is 0.16*g*.

The Tianjing record of Ninghei 1976 earthquake (amplitude *M*6.9, epicentral distance 65*km*, maximum acceleration 0.135*g*) are used as another ground motion input, in which the amplitude is adjusted to 0.05*g*. The computed response spectrum is shown in dashed line in Fig.7. Besides, The EW and UD components of the Taft 1952 earthquake record are used as the third ground motion and the amplitude is scaled to 0.06*g*. The computed response spectrum is shown in dash dot line in Fig.7. The original UD components are used with no changes except the peak values are scaled to 2 / 3 of the horizontal inputs. The responses with these two ground motions are large than the response shown above. The response with Tianjing record is larger than with the Taft record. In these two cases, the maximum moments at the end of pile adjacent to platform are all exceeded the ultimate moment.

The seismic responses of this pier in transverse direction have also been performed with the same three ground motion inputs. The results indicated that the response in transverse direction is small compared to in longitudinal direction. The maximum shear force at the bearing is only about 1 / 3 of at the pier base. This is because the stiffness of this pier in transverse direction is larger than in longitudinal direction. Besides, the maximum moment at the pile end adjacent to platform is about the same with in longitudinal direction.

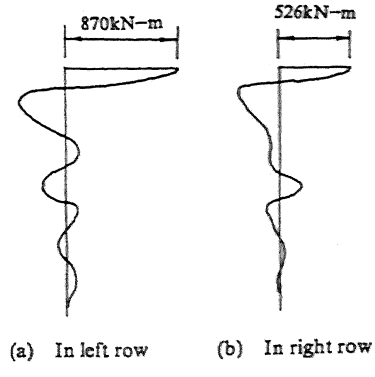

Fig.11 Moment distribution along piles

6 SUMMARY AND CONCLUSIONS

It can be seen that the evaluation results have good agreements with the actual seismic damage appearances. The evaluation results indicated that:

(1) there is a large shear force acting at the bearing in the longitudinal direction during earthquakes. It measures about 4 times of the shear force acting on the pier base and some strengthen steps should be adopted in the design. The pier stiffness, especially the cap stiffness, in longitudinal direction should be increased to about equal to the value in transverse direction;

(2) there is always a stress focus at pile end adjacent to the platform. Some details should be added in design to enhance its earthquake–resistant ability;

(3) it can be seen from this study that the damage is primarily induced by the hysteresis effect since the piles in this pile foundation have low steel ratios, therefor it is necessary to assure the ductility demand of the pile especially in the area adjacent to platform. A least steel ratio demand should be stipulated in the design specifications;

(4) when the liquefaction is taken place, the buckling stability of the pile should not neglected. In this study, it was found that the buckling effect can increase the maximum moment at the end of pile adjacent to platform from 5% to 10%;

(5) it was also found through this study, the detailed analytical model for soil has little effect on the seismic response of structure(pier and pile) compared to other effect considered in this analytical model;

(6) there are four key elements of the ground motions contributed greatly to the overall inelastic seismic response of the soil–pile–pier system. They are the predominant period, the magnitude of the elastic response spectrum, the peak value and the duration of the ground motions.

REFERENCE

Feng Zhiyong 1986. Seismic response analysis of bridge piers on Loess foundation. Presented to the Lanzhou Railway College in partial fulfillment for M. S. Degree.

Feng Zhiyong, Zhu Xi 1991. Elasto–plastic full range analysis of reinforced concrete members with axial and bending loadings. J. Lanzhou Railway College. 10(4). 1–13.

Harrison. H. B 1973. Computer methods in structural analysis. Prentice Hall, New Jersey.

Michael E. Barenberg, Douglas A. Foutch 1986. Inelastic response and damage assessment of reinforced concrete highway bridges subjected to seismic loadings. Structural research series NO. 526. University of Illinois at Urbana–Champaign.

Seismic Design Guidelines for Highway Bridges. ATC–6 1981, Applied Technology Council. Berkeley, CA.

Zhu Xi, Feng Zhiyong 1987. Seismic response analysis of bridge piers on loess foundation. Proc. of International Symposium on Geomechanics, Bridges and Structures. Lanzhou, P. R. China. 639–646.